frontiers | Frontiers in Energy Research

TYPE Original Research
PUBLISHED 23 September 2024
DOI 10.3389/fenrg.2024.1457556

OPEN ACCESS

EDITED BY
Zhaoning Song,
University of Toledo, United States

REVIEWED BY
Yuanhang Cheng,
Nanjing University of Science and Technology, China
Yifan Yin,
University of Toledo, United States

*CORRESPONDENCE
Feng Yan,
fengyan@asu.edu

RECEIVED 01 July 2024
ACCEPTED 10 September 2024
PUBLISHED 23 September 2024

CITATION
Menon H and Yan F (2024) Device simulation and experimental validation of perovskite-cadmium telluride 4T tandem solar cell. *Front. Energy Res.* 12:1457556. doi: 10.3389/fenrg.2024.1457556

Device simulation and experimental validation of perovskite-cadmium telluride 4T tandem solar cell

Harigovind Menon[1] and Feng Yan[2]*

[1]Department of Metallurgical and Materials Engineering, The University of Alabama, Tuscaloosa, AL, United States, [2]School for Engineering of Matter, Transport and Energy, Arizona State University, Tempe, AZ, United States

Developing tandem solar cells is an excellent strategy to break through the Shockley–Queisser (SQ) limit for single-junction solar cells. A major factor in developing a tandem solar cell is to make it cost-efficient with high device performance. Here, we demonstrate the proof of concept of four terminal (4T) tandem solar cell using a perovskite solar cell (PSC) as a wide bandgap (WBG) top cell and narrow bandgap (NBG) cadmium telluride (CdTe) as a bottom cell. A 4T tandem device power conversion efficiency (PCE) exceeding 23% was obtained using SCAPS (solar cell capacitance simulator) simulation, demonstrating the architecture's feasibility. Further, we fabricated two WBG semitransparent perovskite cells with different bandgaps (1.6eV and 1.77eV) and mechanically stacked it with NBG CdTe (1.5eV) to obtain tandem efficiencies of 18.2% and 19.4% respectively. From the results, we concluded that the PSC with a bandgap of 1.77eV is more suitable to be paired with the NBG CdTe solar cell to get good device performance and effective spectral utilization. The experimental results show promising device performance and pave the way to further improve device performance by engineering the device architecture and interfaces.

KEYWORDS

tandem solar cells, perovskite, cadmium telluride, thin film solar cells, SCAPs

1 Introduction

The photovoltaic (PV) industry currently is dominated by single junction (SJ) solar cells that are inherently limited in the power conversion efficiency (PCE) of converting solar energy to electricity due to the theoretical Shockley-Queisser (SQ) limit of 31%–33% (Jošt et al., 2020; Leijtens et al., 2018). One proven approach to break the SJ SQ limit is to form a tandem device by stacking solar cells with different bandgaps, allowing each cell to absorb different parts of the solar spectrum more efficiently by minimizing sub-bandgap and thermalization losses to achieve high PCE (Ho-Baillie et al., 2021; Zhao et al., 2018). The top cell with a wide-bandgap (WBG) absorbs high energy photons and allows the low energy photons to be absorbed by the narrow-bandgap (NBG) bottom cell thus realizing a broader region of wavelength absorption. Theoretical efficiency of around 42% can be achieved for an ideal two-junction tandem solar cell (Shen et al., 2020). The most simple tandem device architecture from a process development point of view is the mechanically stacked four-terminal tandem where the two sub-cells are fabricated independently, stacked on top of each other and contacted individually (Werner et al., 2018; Eperon et al., 2016). This allows for easy fabrication where each cell can be fabricated at the optimum device conditions.

Minimizing parasitic absorption loses and device manufacturing cost are two important conditions to improve the viability of the tandem configuration (Lal et al., 2017; Wali et al., 2018).

Inorganic–organic perovskites are compounds with the ABX_3 formula containing methylammonium iodide (MAI), formamidinium iodide (FAI), Cs or their mixture as A site cation, Pb, Sn, or a mixture of them as divalent metal (B site) and I and/or Br as halide (X site) (Saliba et al., 2016). They have emerged as an extremely promising photovoltaic (PV) technology owing to their rapidly increasing PCE, excellent optoelectronic properties, ease of fabrication and low processing costs (Song et al., 2019; Ramos et al., 2018; Bi et al., 2016). PSCs with its tunable bandgap and low temperature of processing is an ideal candidate to be used in tandem solar cells. Tandem cells have been made with perovskite coupled with Silicon (Albrecht et al., 2016; Ba et al., 2018; Chen et al., 2016; Fan et al., 2017), CIGS (Bailie et al., 2015; Guchhait et al., 2017; Shen et al., 2018), CZTS (Todorov et al., 2014) and other perovskite solar cells (Zhao et al., 2018; Eperon et al., 2015; Zhao et al., 2017; Sheng et al., 2017).

CdTe with its recent improvement in PCE and low cost of fabrication makes it one of the most commercially successful thin film technology (Li et al., 2021; Munshi et al., 2017). CdTe devices offer several advantages like performance stability in warm conditions (Virtuani et al., 2010), high-throughput of manufacturing (Kranz et al., 2013), and very short energy payback time (Kranz et al., 2013; Walker et al., 2022). CdTe has an optimum band gap near 1.5 eV according to the SQ limit so that it could deliver efficiencies around 32%, with an open circuit voltage (Voc) of more than 1 V and a short circuit current density (Jsc) of more than 30 mA/cm^2 (Romeo and Artegiani, 2021). CdTe has been coupled with Si (Enam et al., 2017; Isah et al., 2021; Cheng and Ding, 2021) and CIGS (Weiss, 2021; Noh et al., 2023) for fabricating tandem cells but very less research has been done for pairing it with PSC (Siegler et al., 2019). Paul et al. developed a 4T CdTe perovskite tandem with a WBG PSC with PCE of 19.56% and 19.56% CdTe cell achieving a tandem efficiency of 24.2% (Paul et al., 2024). Yan et al. recently published their work on four-terminal perovskite CdSeTe tandem solar cells with power conversion efficiency exceeding 25% with a PSC in inverted (p-i-n) structure by tuning the bandgap of the WBG PSC from 1.64eV to 1.82eV (Dolia et al., 2024).

Here, we demonstrate a 4T tandem device based on a wide bandgap (WBG) semitransparent perovskite top cell and CdTe narrow bandgap (NBG) bottom cell. We first simulated the 4T tandem solar cell using SCAPS software to understand the feasibility of the design. By pairing a WBG PSC with the CdTe cell, we obtained a 4T Tandem PCE of 23.3% measured under reverse voltage scan under 100 mW/cm^2 1.5G solar irradiation. Then to further corroborate the simulated results with experimental data, we fabricated 4T tandem cells from two WBG PSC (1.77eV and 1.6eV) and CdTe NBG cell and demonstrated that these materials can provide reasonable efficiency in the tandem configuration. Two WBG PSCs were used as top cells to study the effect of bandgap on the following tandem configuration. The champion 4T tandem cell with the top WBG PSC (1.6eV) and bottom CdTe had a PCE of 18.16% compared to the WBG PSC (1.77eV) with a tandem PCE of 19.41%. From the device performance, we conclude that the perovskite material with bandgap of 1.77eV is more suitable for the 4T tandem architecture due to effective spectral utilization and higher PCE. The tandem configuration with 1.6eV is having a PCE close to SJ CdTe solar cell (17.94%) thus limiting its use in the tandem architecture.

2 Experimental section

2.1 SCAPS-1d device simulation

We used SCAPS-1D to model the single junction and tandem solar cells to demonstrate the feasibility of perovskite cadmium telluride four-terminal tandem tandem architecture. SCAPS-1D is utilized to model the single junction and tandem solar cells. SCAPS-1D is an open-source application to simulate solar cells, which was developed by the Department of Electronics and Information Systems (ELIS) at the University of Ghent, Belgium. (Burgelman et al., 2000). The details for the simulation are listed in Table 1 for the materials used in this work.

2.2 WBG PSC precursor preparation

1.6eV WBG PSC: $Cs_{0.04}FA_{0.81}MA_{0.15}PbI_{2.49}Br_{0.51}$: The 1.6eV $Cs_{0.04}FA_{0.81}MA_{0.15}PbI_{2.49}Br_{0.51}$ (1.35M) precursor solution was prepared with corresponding molar ratios of 1.1 M lead iodide (PbI_2), 0.24M lead bromide ($PbBr_2$), 1.05M formamidinium iodide (FAI), 0.2M Methylammonium bromide (MABr), and 0.05M cesium iodide (CsI) dissolved in a mixed solvent of dimethylformamide (DMF) and dimethyl sulfoxide (DMSO) with a volume ratio of 4:1 (Vijayaraghavan et al., 2020). The prepared perovskite precursor was then stirred at room temperature for 3 hours.

1.77eV WBG PSC: $FA_{0.8}Cs_{0.2}Pb(I_{0.7}Br_{0.3})_3$: The 1.77eV $FA_{0.8}Cs_{0.2}Pb(I_{0.7}Br_{0.3})_3$ precursor solution was prepared with corresponding molar ratios of 0.55 mmol PbI_2, 0.45 mmol $PbBr_2$, 0.8 mmol FAI, and 0.2 mmol CsI in 1 nL mixed DMF and DMSO with a volume ratio of 4:1 (Nakamura et al., 2022). The prepared perovskite precursor was then stirred at room temperature for 3 hours.

2.3 Film deposition and device fabrication of WBG PSC

PSCs were fabricated as mentioned in our previous work (Vijayaraghavan et al., 2021). The as-deposited ITO substrates were successively cleaned by sonication with detergent solution, deionized water, acetone, and isopropanol for 30 min followed by a UV-Ozone treatment for 30 min. The SnO_2 electron transport layer (ETL) was spin-coated using the prepared precursor solution. The SnO_2 layers were annealed at 180°C for 1 h in ambient conditions. The ITO substrates were then moved to a nitrogen-filled glovebox for depositing the perovskite layer. The triple cation perovskite was deposited by a two-step spin-coating process. The perovskite precursor was deposited using static deposition. The first step

TABLE 1 Materials parameters used in the simulation.

Parameter	Materials						
	Spiro	PSC	SnO_2	ITO	FTO	CdS	CdTe
Thickness (nm)	250	500	100	100	300	25	300
Bandgap (eV)	3.06	1.6	3.5	3.72	3.6	2.4	1.5
Electron Affinity (eV)	2.2	3.9	4.0	3.6	3.8	4.0	3.9
Dielectric Permittivity	3.0	10	9.0	10	10.0	9.35	9.4
Conduction band of state (cm^{-3})	2.8×10^{19}	2.2×10^{18}	2.2×10^{17}	4×10^{19}	2.2×10^{17}	2.2×10^{18}	8.0×10^{17}
Valence band of states (cm^{-3})	2.2×10^{19}	1.8×10^{18}	2.2×10^{17}	1×10^{18}	1.8×10^{18}	1.8×10^{19}	1.9×10^{18}
Electron Mobility (cm^2/Vs)	1×10^{-4}	1.66	20	30	100	100	30
Hole Mobility (cm^2/Vs)	2×10^{-4}	1.60	10	5.0	25	25	4
Donor Concentration (cm^{-3})	0.0	1.0×10^{9}	1.0×10^{18}	1×10^{9}	1.0×10^{17}	1×10^{18}	0
Acceptor Concentration (cm^{-3})	1.0×10^{18}	1.0×10^{9}	0		0	0	2.0×10^{14}

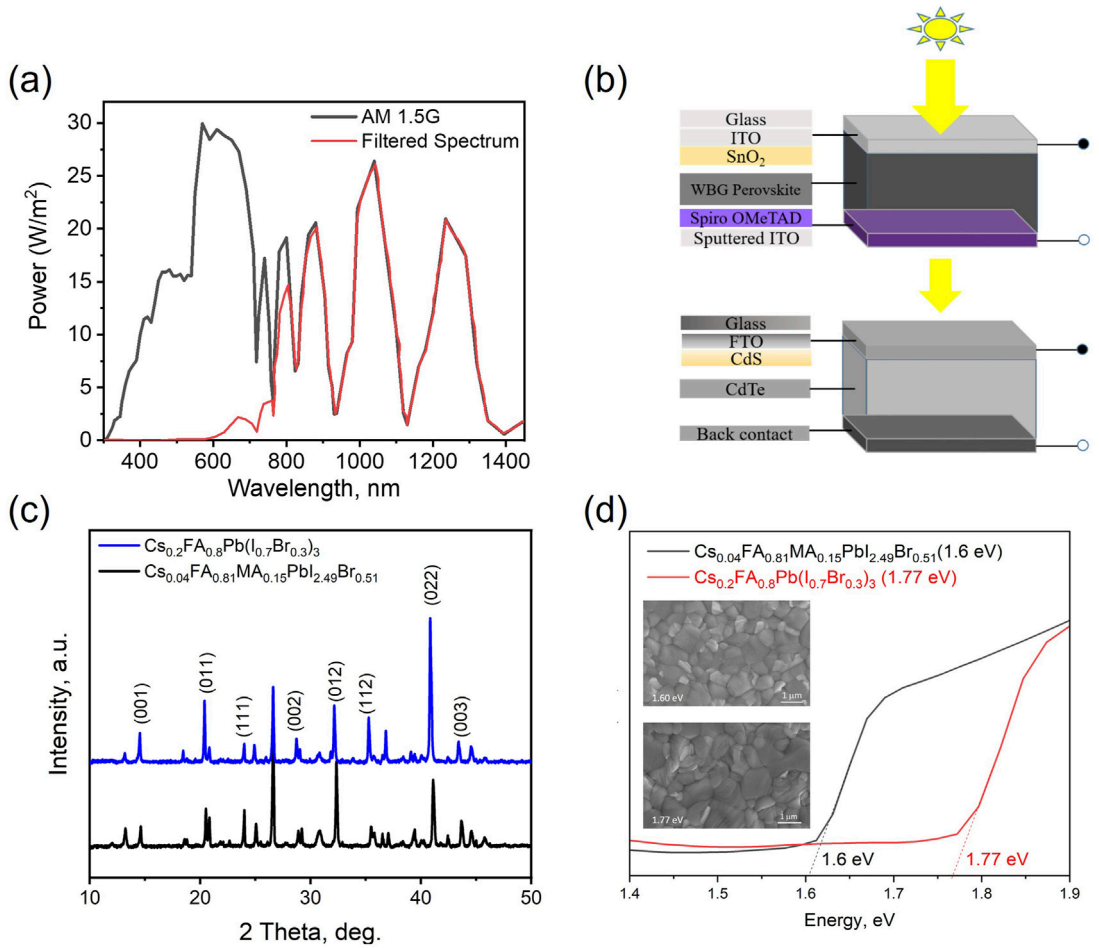

FIGURE 1
(A) The intensity of filtered AM 1.5G spectrum transmitted through the perovskite layer of the top sub-cell; **(B)** proposed device architecture of 4T Tandem cell, **(C)** X-ray diffraction spectra for the 1.6 and 1.77 eV perovskite film, and **(D)** UV-Vis absorbance spectra for the 1.6 and 1.77 eV perovskite with the scanning electron microscopy (SEM) surface morphology as shown in the inset 1.6 eV (top) and 1.77 eV (bottom).

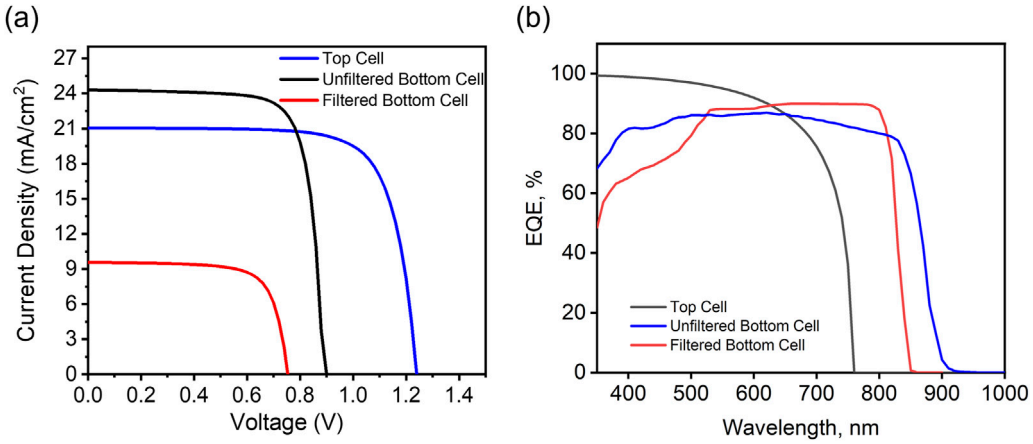

FIGURE 2
SCAPS Simulated tandem perovskite/CdTe device: **(A)** Photocurrent density–voltage and **(B)** External Quantum Efficiency and of the best semitransparent PSC with bandgap of 1.6eV, unfiltered CdTe solar cells, and the filtered CdTe solar cell.

TABLE 2 SCAPS simulated photovoltaic parameters of the WBG PSC cells with a bandgap of 1.6eV, CdTe cells, and the resulting 4T tandem efficiency.

	Voc (V)	Jsc (mA/cm2)	FF (%)	PCE (%)
WBG PSC	1.23	21.05	75	19.62
Unfiltered CdTe	0.89	24.30	77.37	16.68
Filtered CdTe	0.75	9.57	73.10	3.75
4T Tandem Cell				23.37

was at a low speed of 1,000 r.p.m for 10s and then at a high speed of 6,000 r.p.m for 20s. Diethyl ether was dropped on the spinning ITO substrate during high-speed rotation 25s before the end of the spin coating. The films were then annealed at 100°C for 30 minutes. A spiro-OMeTAD hole transport layer (HTL) was deposited on top of the perovskite film by spin coating at 3,000 rpm 30s. Tin-doped indium oxide films were deposited on the film using DC sputtering. The thickness of the ITO was controlled by the deposition time and the sheet resistivity of the ITO was tuned by control of the partial oxygen pressure in the Ar/O_2 mixed gas during sputtering from 0% to 3%. To prevent the bombard effect of the ITO on the spiro-OMeTAD layer, we reduced the power to 10W and tuned the distance between the target and substrate to 15 cm. The deposition thickness was around 50 nm and the sheet resistivity was around 38.2 Ω/Square.

2.4 Film deposition and device fabrication of CdTe cell

CdTe device fabrication details were reported elsewhere. (Montgomery et al., 2019). In brief, the CdTe film was grown using close space sublimation (CSS.) with a CdS buffer layer deposited using chemical bath deposition on the fluorine-doped SnO_2-coated glass substrate. The $CdCl_2$ treatment was performed before the Cu doping using the CuSCN.

2.5 4T-tandem solar cell fabrication

The 4T tandem cell was completed by mechanically stacking the WBG PSC on the NBG CdTe solar cell.

2.6 Materials and device characterization

The electrical characteristics were obtained using a solar simulator (Newport, Oriel Class AAA 94063A, 1000-W Xenon light source) with a Keithley 2,420 source meter under simulated AM 1.5G (100 mW/cm^2) solar irradiation. The masked active area is 0.08 cm^2. The light intensity was calibrated using a silicon reference cell (Newport, 91150V, certified by the National Renewable Energy Lab). The current-voltage scan rate was 100 mVs−1. The masked active area is 0.08 cm2. The external quantum efficiency (EQE) was obtained by an EnliTech QE measurement system. The transmittance of the films was characterized using the UV-Vis (Shimadzu UV-1800).

3 Results and discussions

3.1 SCAPS simulation

SCAPS-1D does not support the simulation of a multi-junction solar cell fully. For the 4T tandem architecture, we first simulated the top cell with the standard AM 1.5G 1 solar spectrum which was followed by the filtration of the incident AM 1.5G spectrum using the model mentioned below using Equation 1. The bottom cell was then simulated using the filtered spectrum from the top cell.

$$S(\lambda) = S_0(\lambda).\exp\left\{\sum_{i=1}^{4} -a\,\mathrm{mati}(\lambda)\mathrm{dmati}\right\} \quad (1)$$

Where S_0 (λ) is the incident A.M 1.5G spectrum, S(λ) is the filtered spectrum from the top cell, a(λ) is the absorption coefficient and mati represents a particular material (i = 1 for Spiro-OMeTAD,

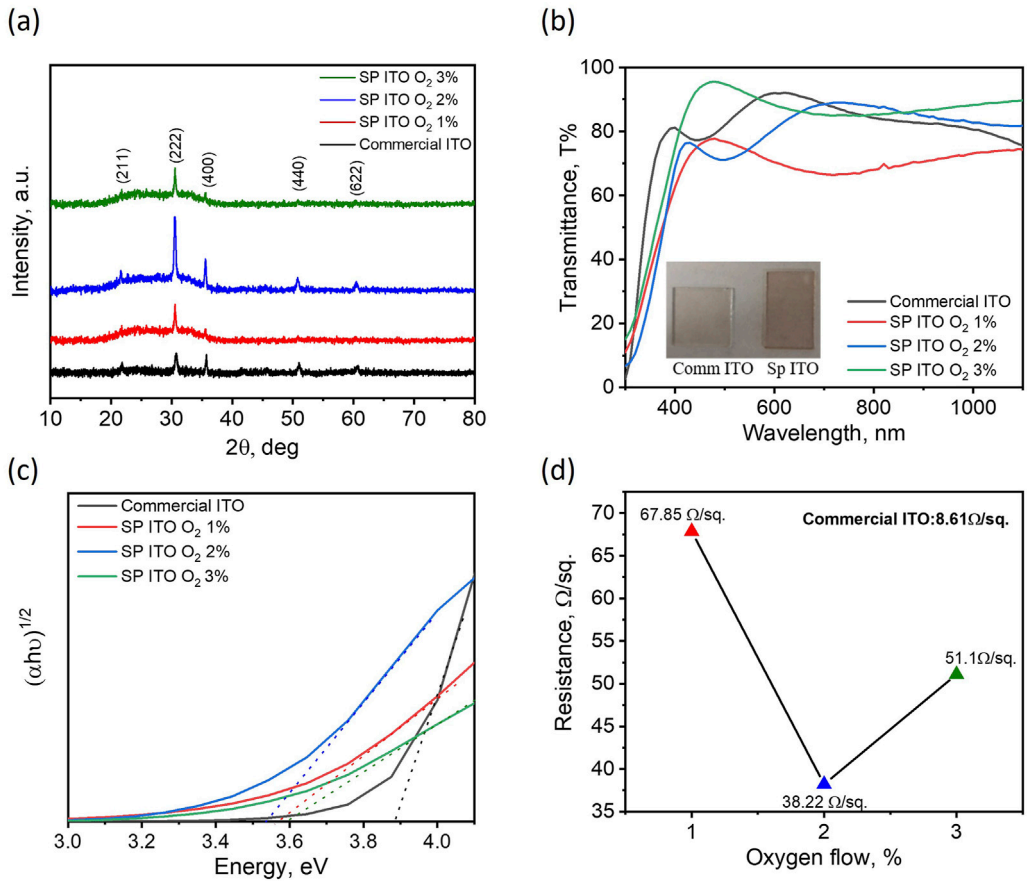

FIGURE 3
Sputtered ITO top electrode characterization for the perovskite/CdTe tandem device by tuning the oxygen partial pressure **(A)** XRD, **(B)** UV-Vis Transmittance, and the **(C)** bandgap and **(D)** sheet resistivity determination.

TABLE 3 Experimental photovoltaic parameters of semitransparent WBG PSC (1.6eV and 1.77eV) cells with CdTe cells, and the resulting 4T tandem efficiencies.

	Voc (V)	Jsc (mA/cm^2)	FF (%)	PCE (%)
1.6eV WBG PSC	1.13	19.01	67.59	14.53
Unfiltered CdTe	0.80	31.46	71.14	17.94
Filtered CdTe	0.74	6.67	73.18	3.63
Tandem PCE				18.16
1.77eV WBG PSC	1.16	15.83	68.8	13
Unfiltered CdTe	0.80	31.46	71.14	17.94
Filtered CdTe	0.74	12.56	68.84	6.41
Tandem PCE				19.41

2 for perovskite material, 3 for SnO_2 and 4 for ITO) for the top perovskite cell and d is the thickness of each layer. Figure 1A shows a plot of the filtered AM1.5G spectrum used to simulate the bottom cell in the tandem configuration.

Figure 1B shows the schematic of the 4T tandem cell with the WBG PSC as the top cell and CdTe as the bottom cell. The XRD for the perovskite film are shown in Figure 1C, and the SEM and UV-Vis absorbance spectra in Tauc plot are shown in Figure 1D. It confirms that the bandgap can be tuned by tailoring the perovskite composition. The WBG PSC has $Cs_{0.04}FA_{0.81}MA_{0.15}PbI_{2.49}Br_{0.51}$ (1.6eV) as the perovskite absorber, SnO_2 as the electron transport layer (ETL) and Spiro OMeTAD as the hole transport layer (HTL) and sputtered indium tin oxide (ITO) as the electrode. The NBG CdTe cell has CdS as the ETL, CdTe as the absorber layer, and carbon as the counter electrode. The SCAPS simulation is performed with the AM1.5G solar spectrum used for the SJ WBG PSC and the filtered spectrum for the NBG CdTe cell. The effective 4T tandem PCE is the sum of the PCE of the WBG PSC and the PCE of the filtered NBG CdTe cell. All the simulations have been performed at a temperature of 300 K. Further, the losses due to the reflection at interfaces as well as the series resistance of the device have not been taken into consideration. Input parameters have been carefully chosen from published literature and experimental works and are listed in Table 1, (Islam et al., 2020; Karthick et al., 2020; Nykyruy et al., 2019).

Figure 2A shows the current density vs. voltage (J-V) curves for the WBG PSC and the CdTe NBG bottom cell. For the 4T configuration, the optimum photovoltaic parameters of the top cell and the bottom cell when the AM 1.5G spectrum and the filtered spectrum respectively are listed in Table 2. Thus, from the simulation for the 4T device design, the champion PCE obtained is

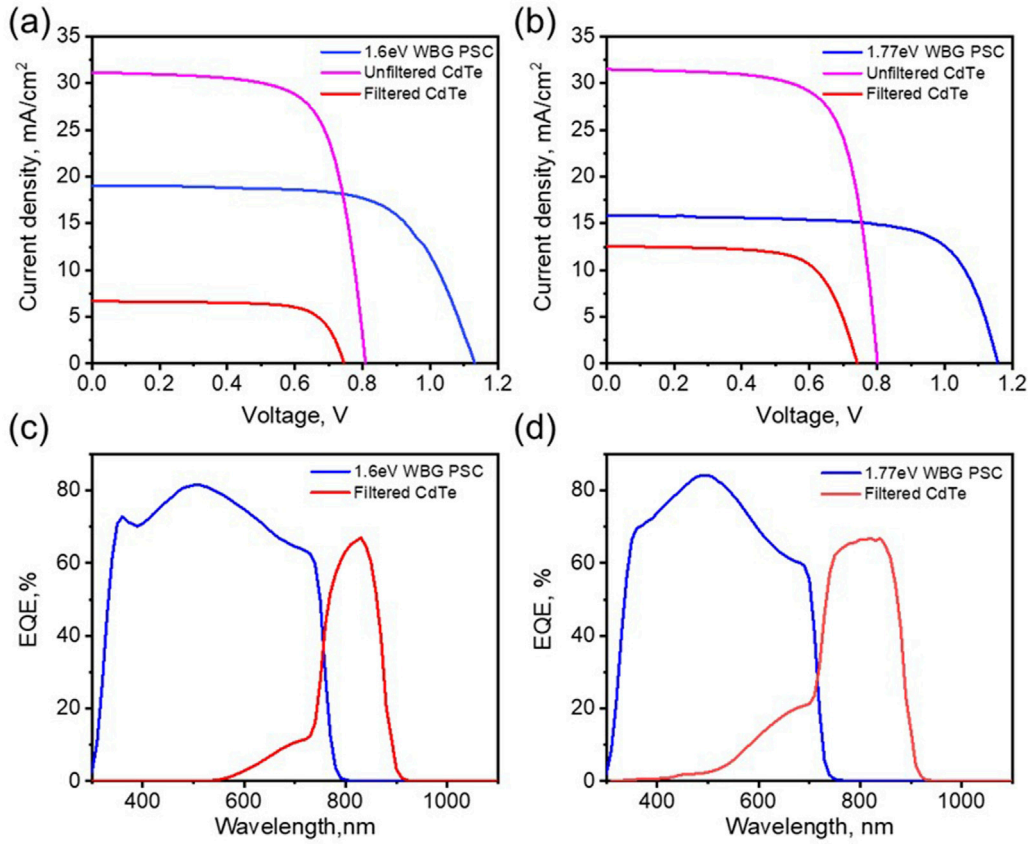

FIGURE 4
Experimental device performance of perovskite/CdTe 4-T device. JV curves of 4T Tandem solar cell with **(A)** 1.6eV WBG PSC top cell and **(B)** 1.77eV WBG PSC top cell. EQE curves of 4T Tandem solar cell with **(C)** 1.6eV WBG PSC top cell and **(D)** 1.77eV WBG PSC top cell.

23.37%, which is higher than either of the individual cells which have a PCE of 19.62% and 16.68% (top and bottom cells, respectively). The WBG PSC absorbs most of the incident light to the bottom cell resulting in lower PCE of the filtered NBG CdTe cell. External quantum efficiency (EQE) performances of the 2 cells are also shown in Figure 2B. The QE plot for the WBG PSC shows that the device exhibits an excellent QE value of 97% up to a wavelength of 550 nm of the incident radiation. The QE of the top sub-cell drops to nearly zero around 770 nm. The EQE was also simulated using the SCAPS for the unfiltered bottom CdTe cells. When the bottom sub-cell is illuminated with the top cell as a filter, the QE is over 70% to 800 nm and reduces to 0% at ~850 nm. This shows that the 4-T tandem device configuration with the WBG PSC cell and the CdTe cell exhibits good overall QE which spans the visible and infrared regions of the electromagnetic spectrum.

The ITO top electrode was deposited using the sputtering system. To minimize the damage of the sputtered ITO on the spiro-OMeTAD hole transport layer, we utilize 10 W and tune the partial pressure to achieve a 38.2 Ω/square sheet resisitivity and the crystalline structure was characterized as shown in the Figure 3A, where the ITO peaks in line with the commercial ITO substrate. In addition, the transmittance of the sputtered ITO was characterized using the UV-Vis transmittance and transparency can reach about 90% by increasing the oxygen partial pressure to 3% in the Ar/O2 mixture gas. The bandgap of the sputtered ITO films was determined via the Tauc plot, as shown in Figure 3C, where the bandgap above 3.5 eV for all these sputtered ITO. The sheet resistivity of these ITO films were characterized using the 4-probe and the lowest sheet resistivity can be 38.2. Ω/square, which is suitable as the top electrode for the tandem perovskite/CdTe device.

To study the impact of optimizing the top cell bandgap for effective spectral utilization, we fabricated two WBG PSCs with a bandgap of 1.6eV and 1.77eV. The top WBG PSC acts as an optical filter for the NBG CdTe cell and absorbs wavelength between 300 and 700 nm, whereas the unabsorbed light, especially those at longer wavelengths, is expected to be harvested by CdTe bottom solar cell. In this work, we used a buffer layer-free semitransparent PSC employing sputtering deposited ITO as a transparent electrode in a device configuration of "glass/ITO/SnO_2/WBG PSC/Spiro OMeTAD/ITO". The JV characteristics of the 4T tandem cell under AM 1.5 G simulated sunlight (100 mW cm^{-2}) are shown in Figure 3 and a summary of the key parameters is also displayed in Table 3.

The PSC with 1.6eV bandgap has a PCE of 14.53% and the filtered NBG CdTe cell has a PCE of 3.63% giving the overall 4T tandem PCE of 18.16%. The PSC with 1.77eV had a PCE of 13% and the filtered NBG CdTe had a PCE of 6.41% giving an overall 4T tandem PCE of 19.41%. The low values of Voc for the WBG PSC compared to the bandgap are mainly attributed to light-induced

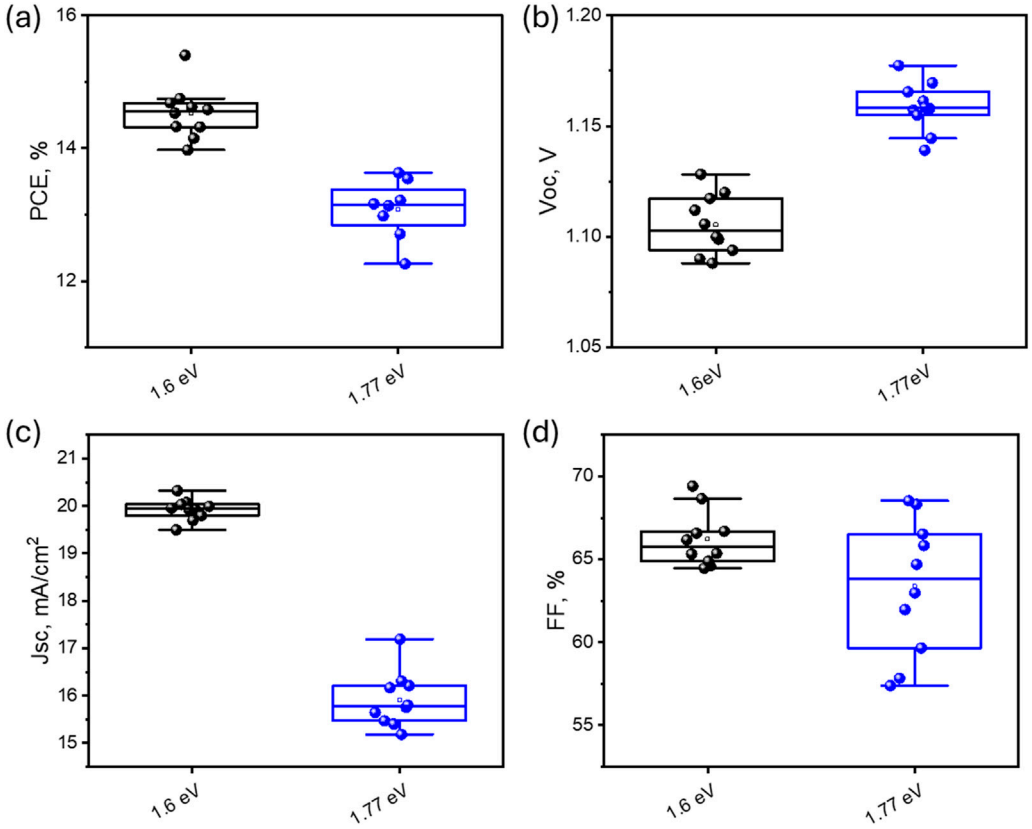

FIGURE 5
Statics of device performance of perovskite solar cell with carbon electrode **(A)** PCE, **(B)** Voc, **(C)** Jsc, and **(D)** FF.

halide segregation. Additional work must be done to mitigate these losses associated with halide segregation to improve cell performance. Here the 4T tandem with WBG PSC of 1.6eV has a PCE very close to the unfiltered CdTe thus limiting its use in the architecture as shown in Figure 4A. The 1.77eV perovskite filter allows for more light to get transmitted to the NBG CdTe thus generating improved filtered PCE as shown in Figure 4B. To analyze the wavelength-dependent spectral application, we compare the EQE of best performing tandem device (Figures 4C, D). The top cell displays onset wavelength of 760 nm, whereas the bottom cell exhibits an onset wavelength of 900 nm. Due to the close bandgap between the 2 cells, there can be further improvement in the spectral utilization. Improved spectral optimization can be obtained by increasing the bandgap of the WBG perovskite but this would lead to lower PCE of the WBG PSC. Thus it is a tradeoff between effective spectral utilization and improving the overall tandem performance. The statics of device performance for both 1.6 eV and 1.77 eV perovskite are shown in Figure 5. The overall device performance still needs to be further optimized. The Fill factor should be further improved by improving the back contact from the carbon to the metal electrode.

We observe that the PV parameters obtained in the experiments are close to the simulated results, but the simulated results are higher. For example, the Voc simulated in this work is slightly higher than the experimental results. This could be due to the fact that we are not considering the losses associated with halide segregation in the simulated work. Also, we have not considered series and shunting loses in the simulated results. Therefore, this difference in voltage and current explains the difference observed in FF and PCE.

In summary, we demonstrate a 4T tandem solar cell based on WBG PSC and NBG CdTe cells. From the simulation, we demonstrated the possibility of forming a 4T tandem cell with PCE exceeding 23%. We then experimentally fabricated two WBG PSC with bandgaps of 1.6eV and 1.77eV and on pairing with the CdTe cell, we demonstrated PCE of 18.16% and 19.41% respectively. From the results, the WBG PSC with 1.77eV is more tuned to be used in configuration with the CdTe cell due to improved spectral utilization. Further work has to be done to find the exact tradeoff between the WBG PSC performance and the effective spectral utilization in the tandem cell to improve the overall PCE. We also have to do additional work on addressing the issue associated with light-induced halide segregation in WBG PSC to further improve the device performance and to get a device performance closer to the simulated results.

The study of tandem device structure for improving the device performance shall be an effective way towards high-efficiency CdTe solar cells. This research also suggests that CdTe would be a suitable NBG candidate for the fabrication of tandem solar cells with WBG-absorbing materials like PSC.

Data availability statement

The raw data supporting the conclusions of this article will be made available by the authors, without undue reservation.

Author contributions

HM: Data curation, Formal Analysis, Investigation, Methodology, Writing–original draft. FY: Data curation, Formal Analysis, Investigation, Methodology, Writing–original draft, Conceptualization, Funding acquisition, Project administration, Resources, Software, Supervision, Validation, Visualization, Writing–review and editing.

Funding

The author(s) declare that financial support was received for the research, authorship, and/or publication of this article. This work is supported by the National Science Foundation under contract No. ECCS-2413632, MOMS-2330728, TI-2329871, and DMR-2330738, and CMMI-2226918, and DMREF-2323766. This journal article was developed based upon funding from the Alliance for Sustainable Energy, LLC, Managing and Operating Contractor for the National Renewable Energy Laboratory for the U.S. Department of Energy.

Conflict of interest

The authors declare that the research was conducted in the absence of any commercial or financial relationships that could be construed as a potential conflict of interest.

The authors declare that this study received funding from Alliance for Sustainable Energy, LLC . The funder had the following involvement in the study: CdTe solar cell study.

Publisher's note

References

Albrecht, S., Saliba, M., Correa Baena, J. P., Lang, F., Kegelmann, L., Mews, M., et al. (2016). Monolithic perovskite/silicon-heterojunction tandem solar cells processed at low temperature. *Energy & Environ. Sci.* 9 (1), 81–88. doi:10.1039/c5ee02965a

Ba, L., Liu, H., and Shen, W. (2018). Perovskite/c-Si tandem solar cells with realistic inverted architecture: achieving high efficiency by optical optimization. *Prog. Photovoltaics Res. Appl.* 26 (11), 924–933. doi:10.1002/pip.3037

Bailie, C. D., Christoforo, M. G., Mailoa, J. P., Bowring, A. R., Unger, E. L., Nguyen, W. H., et al. (2015). Semi-transparent perovskite solar cells for tandems with silicon and CIGS. *Energy & Environ. Sci.* 8 (3), 956–963. doi:10.1039/c4ee03322a

Bi, D., Yi, C., Li, X., Luo, J., Decoppet, J-D., Zhang, F., et al. (2016). Polymer-templated nucleation and crystal growth of perovskite films for solar cells with efficiency greater than 21. *Nat. Energy* 1 (10), 1–5. doi:10.1038/nenergy.2016.142

Burgelman, M., Nollet, P., and Degrave, S. (2000). Modelling polycrystalline semiconductor solar cells. *Thin solid films* 361, 527–532. doi:10.1016/s0040-6090(99)00825-1

Chen, B., Bai, Y., Yu, Z., Li, T., Zheng, X., Dong, Q., et al. (2016). Efficient semitransparent perovskite solar cells for 23.0%-efficiency perovskite/silicon four-terminal tandem cells. *Adv. Energy Mater.* 6 (19), 1601128. doi:10.1002/aenm.201601128

Cheng, Y., and Ding, L. (2021). Perovskite/Si tandem solar cells: fundamentals, advances, challenges, and novel applications. *SusMat* 1 (3), 324–344. doi:10.1002/sus2.25

Dolia, K., Neupane, S., Fu, S., Yin, Y., Abudulimu, A., Rahimi, A., et al. (2024). Four-terminal perovskite-CdSeTe tandem solar cells: from 25% toward 30% power conversion efficiency and beyond. *Sol. RRL*. doi:10.1002/solr.202400148

Enam, F., Rahman, K., Kamaruzzaman, M., Sobayel, K., Chelvanathan, P., Bais, B., et al. (2017). Design prospects of cadmium telluride/silicon (CdTe/Si) tandem solar cells from numerical simulation. *Optik* 139, 397–406. doi:10.1016/j.ijleo.2017.03.106

Eperon, G. E., Leijtens, T., Bush, K. A., Prasanna, R., Green, T., Wang, J. T. W., et al. (2016). Perovskite-perovskite tandem photovoltaics with optimized band gaps. *Science* 354 (6314), 861–865. doi:10.1126/science.aaf9717

Eperon, G. E., Paternò, G. M., Sutton, R. J., Zampetti, A., Haghighirad, A. A., Cacialli, F., et al. (2015). Inorganic caesium lead iodide perovskite solar cells. *J. Mater. Chem. A* 3 (39), 19688–19695. doi:10.1039/c5ta06398a

Fan, R., Zhou, N., Zhang, L., Yang, R., Meng, Y., Li, L., et al. (2017). Toward full solution processed perovskite/Si monolithic tandem solar device with PCE exceeding 20%. *Sol. RRL* 1 (11), 1700149. doi:10.1002/solr.201700149

Guchhait, A., Dewi, H. A., Leow, S. W., Wang, H., Han, G., Suhaimi, F. B., et al. (2017). Over 20% efficient CIGS–perovskite tandem solar cells. *ACS Energy Lett.* 2 (4), 807–812. doi:10.1021/acsenergylett.7b00187

Ho-Baillie, A. W., Zheng, J., Mahmud, M. A., Ma, F. J., McKenzie, D. R., and Green, M. A. (2021). Recent progress and future prospects of perovskite tandem solar cells. *Appl. Phys. Rev.* 8 (4), 041307. doi:10.1063/5.0061483

Isah, M., Rahman, K., Doroody, C., Harif, M., Rosly, H., Sopian, K., et al. (2021). Design optimization of CdTe/Si tandem solar cell using different transparent conducting oxides as interconnecting layers. *J. Alloys Compd.* 870, 159351. doi:10.1016/j.jallcom.2021.159351

Islam, M. T., Jani, M. R., Al Amin, S. M., Sami, M. S. U., Shorowordi, K. M., Hossain, M. I., et al. (2020). Numerical simulation studies of a fully inorganic Cs2AgBiBr6 perovskite solar device. *Opt. Mater.* 105, 109957. doi:10.1016/j.optmat.2020.109957

Jošt, M., Kegelmann, L., Korte, L., and Albrecht, S. (2020). Monolithic perovskite tandem solar cells: a review of the present status and advanced characterization methods toward 30% efficiency. *Adv. Energy Mater.* 10 (26), 1904102. doi:10.1002/aenm.201904102

Karthick, S., Velumani, S., and Bouclé, J. (2020). Experimental and SCAPS simulated formamidinium perovskite solar cells: a comparison of device performance. *Sol. Energy* 205, 349–357. doi:10.1016/j.solener.2020.05.041

Kranz, L., Gretener, C., Perrenoud, J., Schmitt, R., Pianezzi, F., La Mattina, F., et al. (2013). Doping of polycrystalline CdTe for high-efficiency solar cells on flexible metal foil. *Nat. Commun.* 4 (1), 2306–2307. doi:10.1038/ncomms3306

Lal, N. N., Dkhissi, Y., Li, W., Hou, Q., Cheng, Y., and Bach, U. (2017). Perovskite tandem solar cells. *Adv. Energy Mater.* 7 (18), 1602761. doi:10.1002/aenm.201602761

Leijtens, T., Bush, K. A., Prasanna, R., and McGehee, M. D. (2018). Opportunities and challenges for tandem solar cells using metal halide perovskite semiconductors. *Nat. Energy* 3 (10), 828–838. doi:10.1038/s41560-018-0190-4

Li, D.-B., Yao, C., Vijayaraghavan, S. N., Awni, R. A., Subedi, K. K., Ellingson, R. J., et al. (2021). Low-temperature and effective *ex situ* group V doping for efficient polycrystalline CdSeTe solar cells. *Nat. Energy* 6 (7), 715–722. doi:10.1038/s41560-021-00848-z

Montgomery, A., Guo, L., Grice, C., Awni, R. A., Saurav, S., Li, L., et al. (2019). Solution-processed copper (I) thiocyanate (CuSCN) for highly efficient CdSe/CdTe thin-film solar cells. *Prog. Photovoltaics Res. Appl.* 27 (8), 665–672. doi:10.1002/pip.3136

Munshi, A. H., Kephart, J., Abbas, A., Raguse, J., Beaudry, J. N., Barth, K., et al. (2017). Polycrystalline CdSeTe/CdTe absorber cells with 28 mA/cm 2 short-circuit current. *IEEE J. Photovoltaics* 8 (1), 310–314. doi:10.1109/jphotov.2017.2775139

Nakamura, M., Lin, C. C., Nishiyama, C., Tada, K., Bessho, T., and Segawa, H. (2022). Semi-transparent perovskite solar cells for four-terminal perovskite/CIGS tandem solar cells. *ACS Appl. Energy Mater.* 5 (7), 8103–8111. doi:10.1021/acsaem.2c00620

Noh, M. F. M., Arzaee, N. A., Fat, C. C., Tiong, S. K., Teridi, M. A. M., and Zuhdi, A. W. M. (2023). Perovskite/CIGS tandem solar cells: progressive advances from technical perspectives. *Mater. Today Energy*, 101473. doi:10.1016/j.mtener.2023.101473

Nykyruy, L., Yavorskyi, R., Zapukhlyak, Z., Wisz, G., and Potera, P. (2019). Evaluation of CdS/CdTe thin film solar cells: SCAPS thickness simulation and analysis of optical properties. *Opt. Mater.* 92, 319–329. doi:10.1016/j.optmat.2019.04.029

Paul, A., Singha, A., Hossain, K., Gupta, S., Misra, M., Mallick, S., et al. (2024). 4-T CdTe/perovskite thin film tandem solar cells with efficiency >24%. *ACS Energy Lett.* 9, 3019–3026. doi:10.1021/acsenergylett.4c01118

Ramos, F. J., Jutteau, S., Posada, J., Bercegol, A., Rebai, A., Guillemot, T., et al. (2018). Highly efficient MoOx-free semitransparent perovskite cell for 4 T tandem application improving the efficiency of commercially-available Al-BSF silicon. *Sci. Rep.* 8 (1), 16139–16211. doi:10.1038/s41598-018-34432-5

Romeo, A., and Artegiani, E. (2021). CdTe-based thin film solar cells: past, present and future. *Energies* 14 (6), 1684. doi:10.3390/en14061684

Saliba, M., Matsui, T., Seo, J. Y., Domanski, K., Correa-Baena, J. P., Nazeeruddin, M. K., et al. (2016). Cesium-containing triple cation perovskite solar cells: improved stability, reproducibility and high efficiency. *Energy & Environ. Sci.* 9 (6), 1989–1997. doi:10.1039/c5ee03874j

Shen, H., Duong, T., Peng, J., Jacobs, D., Wu, N., Gong, J., et al. (2018). Mechanically-stacked perovskite/CIGS tandem solar cells with efficiency of 23.9% and reduced oxygen sensitivity. *Energy & Environ. Sci.* 11 (2), 394–406. doi:10.1039/c7ee02627g

Shen, H., Walter, D., Wu, Y., Fong, K. C., Jacobs, D. A., Duong, T., et al. (2020). Monolithic perovskite/Si tandem solar cells: pathways to over 30% efficiency. *Adv. Energy Mater.* 10 (13), 1902840. doi:10.1002/aenm.201902840

Sheng, R., Hörantner, M. T., Wang, Z., Jiang, Y., Zhang, W., Agosti, A., et al. (2017). Monolithic wide band gap perovskite/perovskite tandem solar cells with organic recombination layers. *J. Phys. Chem. C* 121 (49), 27256–27262. doi:10.1021/acs.jpcc.7b05517

Siegler, T. D., Shimpi, T. M., Sampath, W. S., and Korgel, B. A. (2019). Development of wide bandgap perovskites for next-generation low-cost CdTe tandem solar cells. *Chem. Eng. Sci.* 199, 388–397. doi:10.1016/j.ces.2019.01.003

Song, Z., Chen, C., Awni, R. A., Zhao, D., and Yan, Y. (2019). Wide-bandgap, low-bandgap, and tandem perovskite solar cells. *Semicond. Sci. Technol.* 34 (9), 093001. doi:10.1088/1361-6641/ab27f7

Todorov, T., Gershon, T., Gunawan, O., Sturdevant, C., and Guha, S. (2014). Perovskite-kesterite monolithic tandem solar cells with high open-circuit voltage. *Appl. Phys. Lett.* 105 (17), 173902. doi:10.1063/1.4899275

Vijayaraghavan, S., Wall, J., Li, L., Xing, G., Zhang, Q., and Yan, F. (2020). Low-temperature processed highly efficient hole transport layer free carbon-based planar perovskite solar cells with SnO2 quantum dot electron transport layer. *Mater. Today Phys.* 13, 100204. doi:10.1016/j.mtphys.2020.100204

Vijayaraghavan, S., Wall, J., Menon, H. G., Duan, X., Guo, L., Amin, A., et al. (2021). Interfacial engineering with NiOx nanofibers as hole transport layer for carbon-based perovskite solar cells. *Sol. Energy* 230, 591–597. doi:10.1016/j.solener.2021.10.039

Virtuani, A., Pavanello, D., and Friesen, G. (2010). "Overview of temperature coefficients of different thin film photovoltaic technologies," in 25th European photovoltaic solar energy conference and exhibition/5th World conference on photovoltaic energy conversion, Freiburg, Germany, September 23–25, 2013.

Wali, Q., Elumalai, N. K., Iqbal, Y., Uddin, A., and Jose, R. (2018). Tandem perovskite solar cells. *Renew. Sustain. Energy Rev.* 84, 89–110. doi:10.1016/j.rser.2018.01.005

Walker, T., Stuckelberger, M. E., Nietzold, T., Mohan-Kumar, N., Ossig, C., Kahnt, M., et al. (2022). The nanoscale distribution of copper and its influence on charge collection in CdTe solar cells. *Nano Energy* 91, 106595. doi:10.1016/j.nanoen.2021.106595

Weiss, D. N. (2021). Tandem solar cells beyond perovskite-silicon. *Joule* 5 (9), 2247–2250. doi:10.1016/j.joule.2021.08.009

Werner, J., Niesen, B., and Ballif, C. (2018). Perovskite/silicon tandem solar cells: marriage of convenience or true love story? An overview. *Adv. Mater. Interfaces* 5 (1), 1700731. doi:10.1002/admi.201700731

Zhao, D., Wang, C., Song, Z., Yu, Y., Chen, C., Zhao, X., et al. (2018). Four-terminal all-perovskite tandem solar cells achieving power conversion efficiencies exceeding 23%. *ACS Energy Lett.* 3 (2), 305–306. doi:10.1021/acsenergylett.7b01287

Zhao, D., Yu, Y., Wang, C., Liao, W., Shrestha, N., Grice, C. R., et al. (2017). Low-bandgap mixed tin–lead iodide perovskite absorbers with long carrier lifetimes for all-perovskite tandem solar cells. *Nat. Energy* 2 (4), 17018–17027. doi:10.1038/nenergy.2017.18